Journal of Power Sources, 8 (1982) 175 - 196

CRYSTALLINE PHASE COMPOSITION OF POSITIVE PLATES IN LEAD/ACID TRACTION BATTERIES UNDER SIMULATED ELECTRIC VEHICLE SERVICE

K. HARRIS, R. J. HILL and D. A. J. RAND

CSIRO Division of Mineral Chemistry, P. O. Box 124, Port Melbourne, Victoria 3207 (Australia)

Summary

A rapid, accurate, and non-destructive X-ray-diffraction (XRD) technique, based on the direct-comparison (or matrix-flushing) method, has been developed for the routine crystalline phase analysis of positive plates from lead/acid batteries.

Analysis has shown that less than 45% of the total positive plate active mass is utilized during battery operation under simulated electric-vehicle service. Although individual plates within a given battery develop different compositions under such conditions, a positive correlation exists between the initial α-PbO_2:β-PbO_2 ratio and the battery cycle life. The α-PbO_2 content initially decreases, then levels off to about half the original amount.

The exact nature of plate failure in test batteries has not been resolved, but XRD studies provide strong evidence that grid passivation by sulphate films is a key factor. Other life-limiting phenomena include electrochemical inactivation of both α- and β-PbO_2 and breakdown of the α-PbO_2 microstructure.

Introduction

Both the capacity and the cycle life of lead/acid traction batteries are strongly dependent on the performance of the positive plate. In the charged condition, the positive plate consists of lead dioxide supported on a lead-alloy grid. The lead dioxide is known to exist in two well characterized modifications, α-PbO_2 and β-PbO_2. The α form has an orthorhombic structure related to that of columbite, and the β form has the tetragonal structure of rutile. Both structures consist of Pb(IV) ions at the centres of distorted octahedra formed by close-packed layers of oxygen ions. In α-PbO_2, the neighbouring octahedra share edges to form zigzag chains, whilst in β-PbO_2 linear edge-shared chains occur [1]. The β form occurs in nature as

0378-7753/82/0000-0000/$02.75

the mineral plattnerite, but no natural occurrence of the α form has been reported. The laboratory synthesis of α-PbO_2 was first described in 1946 [2]. The α form is precipitated electrochemically in a neutral or alkaline environment, the β form in an acidic environment.

Many workers [3 - 22] have identified α-PbO_2 in the anodic corrosion products of lead and its alloys in sulphuric acid. Following these studies, it is now generally agreed that the corrosion product is a multiphase system consisting of β-PbO_2 on the outside of the film facing the electrolyte and PbO_x — where x varies from 1 (tet-PbO) to 2 (α-PbO_2) — in the inner region adjacent to the metal surface. Thus, corrosion of the supporting grid provides a source of α-PbO_2 in the interior of lead/acid battery plates.

The presence of α-PbO_2 in the active material of positive plates of lead/acid batteries was first detected by Bode and Voss [23]. Dodson [24] later showed that the ratio of α-PbO_2 to β-PbO_2 in the formed active material depends on the manufacturing conditions, *e.g.*, the positive paste density (pore volume), the specific gravity and temperature of the formation acid, the rate of formation, etc. More recent studies on commercial plates have suggested [25, 26] the presence of an additional, amorphous form of PbO_2. Caulder *et al.* have also hypothesized [27 - 29] that an "inactive" type of PbO_2 develops in increasing amounts during charge/discharge cycling and results in a decrease in plate capacity. The identity of inactive PbO_2, the mechanism by which it forms, and an explanation for its ineffectiveness in reacting to give lead sulphate during discharge have yet to be established.

The distribution of α- and β-PbO_2 in positive plates has been studied by various authors [30 - 35]. These investigations have shown that whereas β-PbO_2 predominates in the outer surface layers of plates, the inner zones may contain appreciable amounts, *e.g.*, up to 47 wt.% [31, 33] of the α form. Since α-PbO_2 is preferentially formed in less acidic solutions, it has been proposed [24, 35 - 38] that the initial ratio of α- to β-PbO_2 upon plate formation is influenced by local pH changes brought about by diffusion processes within the plate. Ikari *et al.* [11] have shown that the factors promoting a high pH through the restriction of acid to the interior of the plate include a dense coating of lead sulphate on the plate surface, a dilute forming electrolyte, a high PbO content in cured material, and a high paste density.

Differences have been observed in both the electrochemical and the morphological properties of α- and β-PbO_2, and this has encouraged efforts to relate plate performance to the relative amounts of the two species in the positive active material. The β form has been found [24, 30, 32, 39 - 46] to provide more capacity per unit weight during discharge, whereas the α form is believed [36, 47 - 50] to extend the cycle life of positive plates by imparting greater mechanical strength to the structure of the active material. Direct evidence of a possible beneficial effect of α-PbO_2 was demonstrated by Dodson [40], who tested plates containing large amounts of α-PbO_2 and found that they slightly outlasted plates without α-PbO_2. It has, however, been suggested [51] that any beneficial effect will not be very

enduring since α-PbO_2, after conversion to $PbSO_4$ during battery discharge, reverts to the β form upon battery recharge [7, 8, 11, 23, 24, 39, 41, 46].

In view of the important roles of α- and β-PbO_2 in the performance of lead/acid batteries, we have developed a sensitive X-ray-diffraction (XRD) technique for accurate quantitative phase analysis of the crystalline components in positive plates. Although the literature abounds with phase analyses of the positive active material present during both the formation and the cycling of automotive (SLI) and stationary batteries [23 - 25, 40, 46, 52 - 58], little information is available on compositional changes in batteries designed specifically for traction applications. Differences are expected with this type of battery because of the different plate geometry, paste preparation and density, rate and depth of discharge, mode of charge, etc. In this paper, we give details of the XRD technique developed in our laboratory and present initial results obtained for batteries subjected to simulated electric-vehicle duty cycles.

The XRD technique

Most of the previous phase analyses of positive plates in lead/acid batteries use the first of the following four basic XRD methods: (i) simple correlation of the diffracted peak height with the amount of the phase present, (ii) the internal (or external) standard method [59], (iii) the doping method [60, 61], and (iv) the direct-comparison [62], or matrix-flushing, method [63].

In the present study, our objective was to develop an accurate, rapid, and non-destructive technique for analyzing large numbers of necessarily small samples taken from the positive plates of lead/acid batteries at various stages of their cycle life. The method finally chosen, and described in detail below, is a further development of the direct-comparison technique. This technique offers several advantages over the previously used methods:

(1) No internal standard is added. This means that the sample is not contaminated and can therefore be used for microscope examination, chemical analysis, thermal decomposition study, etc. Furthermore, since weighing errors do not have to be considered, the amount of sample removed can be kept to a minimum, with negligible effects on battery operation. Also, the possible conversion of β-PbO_2 to α-PbO_2 [25] during the milling required for sample homogenization is avoided.

(2) Calculated, rather than experimental, calibration constants are applied. This eliminates the usual uncertainty associated with materials chosen as calibration standards in terms of degree of crystallinity, microabsorption, extinction, particle size, and lattice distortion [64].

(3) The effects of preferred orientation [65] are minimized by the measurement of the intensities of groups of four reflections, rather than a single peak, for each phase.

(4) Rapid turnaround is facilitated by the measurement of integrated peak intensities with an automatic step-scan procedure, and by the batch processing of the punched-tape output on a computer.

(5) Although only three-phase mixtures of the lead dioxides and sulphate are discussed in the present study, the method has been used for simultaneous phase determinations of five-component mixtures of α- and β-PbO, α- and β-PbO_2, and $PbSO_4$. The method can also be adapted for the corresponding analysis of Pb and $PbSO_4$ in negative plates.

Theory and method of phase analysis

If W_i and I_i are the weight percentage and X-ray intensity (for a particular plane or set of planes) of phase i in a mixture, and if W_j and I_j are the corresponding quantities for phase j, then a "normalization" constant NC_i exists [63, 65] such that

$$NC_i = (W_j/W_i)(I_i/I_j). \tag{1}$$

This constant is the ratio of the absolute intensities of the two sets of diffraction peaks under consideration, and it can be obtained by calculating from the known structural parameters of the compounds or by measuring the corresponding observed intensities from mixtures of known composition. If appropriate NC_i values are obtained relative to a particular "reference" phase j (β-PbO_2 in the present case) for the $n - 1$ other phases in the mixture, then the weight percentages of these phases in samples of unknown composition can be obtained from the relationship

$$W_i = (I_i/NC_i)\left[\sum_{i=1}^{n}(I_i/NC_i)\right]^{-1}. \tag{2}$$

Because of the well known problems associated with purity, crystallinity, crystal size, and degree of preferred orientation of prepared samples of lead dioxides, especially in relation to the determination of their XRD properties [25, 53, 55, 64, 66, 67], we decided to use *calculated* normalization constants as determined from the calculated diffraction patterns of 50:50 (by weight) binary mixtures of β-PbO_2 with α-PbO_2 or $PbSO_4$. These calculated patterns of two-phase mixtures are displayed in Fig. 1. They provide a convenient basis for discussing the experimental procedure used for phase analysis of the battery plate material.

After an extensive series of trials, a compromise was reached between the length of diffraction record required to give a sufficient number of intense peaks from each phase and the time to achieve a reasonable turnaround in the subsequent phase analyses. The powder patterns given in Fig. 1 and Table 1 were therefore calculated (and subsequently scanned) over the 2θ range 20.0 - 44.3°, using a local version of the Rietveld [68] powder diffraction profile refinement program modified by Wiles and Young [69] to accommodate two phases and two wavelengths (X-ray or neutron). Parameters for the unit cell and the thermal vibration and position of the atoms were determined from neutron powder diffraction data [70]

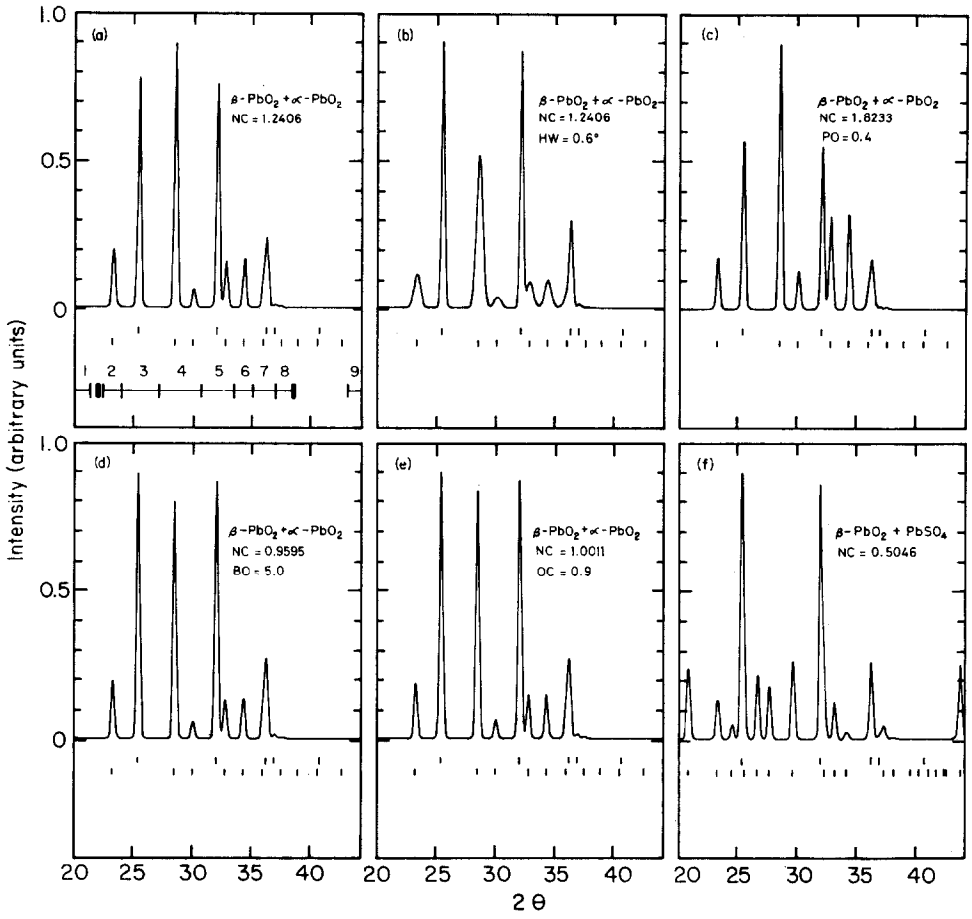

Fig. 1. Calculated X-ray diffraction patterns for 50:50 (by weight) mixtures of β-PbO_2 with α-PbO_2 or $PbSO_4$, together with their associated normalization constants (*NC*). Except where otherwise indicated, the patterns are calculated with a peak width at half-peak-height (*HW*) of 0.3°, a preferred orientation (*PO*) of zero, atom site occupancies (*OC*) of 1.0, and an overall thermal vibration factor (*BO*) of 0.0.

for near-stoichiometric, chemically prepared α- and β-PbO_2, and from single-crystal X-ray data [71] for $PbSO_4$. Except where otherwise indicated, the patterns were calculated for Gaussian peak profiles with a peak width at half-peak-height (*HW*) of 0.3°, a preferred orientation (*PO*) of zero, atom site occupancies (*OC*) of 1.0, and an overall thermal vibration factor (*BO*) of 0.0. The upper and lower rows of vertical lines under each pattern in Fig. 1 represent the positions of all possible Bragg peaks (calculated for copper $K\alpha_1$ radiation) for, respectively, the first- and second-mentioned compounds in each pattern.

Note that the intensities of the peaks in the 2θ range 38.8 - 43.3° have been omitted from the patterns since this region contains many low-intensity

TABLE 1

Miller indices and their calculated and observed relative intensities for the 2θ ranges scanned during the phase analysis procedure

Scanning region	2θ range (°)	β-PbO_2[a]			α-PbO_2[b]			$PbSO_4$[c]		
		(*hkl*)	I_{calc}	I_{obs}	(*hkl*)	I_{calc}	I_{obs}	(*hkl*)	I_{calc}	I_{obs}
1	20.01 - 21.60							(101) (020)	59.9	54.2
2	22.50 - 24.10				(110)	20.9	17.4	(111)	30.5	28.3
3	24.11 - 27.22	(110)	104.3	103.0				(120) (200) (021)	78.0	77.2
4	27.23 - 30.89				(111) (020)	100.0	100.0	(210) (121)	100.0	100.0
5	30.90 - 33.65	(011)	100.0	100.0	(002)	16.8	17.0	(211) (002) (220)	50.4	55.7
6	33.66 - 35.09				(021)	18.2	16.1	(130)	6.0	5.6
7	35.10 - 37.10	(020) (111)	31.8	34.0	(200)	10.6	11.3			
8[d]	37.11 - 38.55				(102)	0.5	0.0	(112) (221) (131)	11.7	12.6
9	43.30 - 44.30							(212) (311)	58.4	68.8

[a]Univar Analytical Reagent.
[b]Prepared by oxidation of β-PbO at 340 °C [66].
[c]Unilab Laboratory Reagent.
[d]This scanning region was used as an additional determination of the $PbSO_4$ content in those cases where the α-PbO_2 content was negligible.

overlapping peaks (Fig. 1(f)) and was skipped during the scanning procedure. The remainder of the record between 20.0 and 44.3° was divided into nine discrete scanning regions (regions 1 - 9, Fig. 1(a) and Table 1) for peak intensity measurements, as well as two regions (the thick bars in Fig. 1(a)) for background determinations (assumed to be linear). For mixtures of the three phases, seven of the nine scanning regions contain overlapping peaks from two or more phases. The remaining two regions (1 and 9 in Fig. 1(a) and Table 1) contain peaks only from $PbSO_4$ (Fig. 1(f) and Table 1) and were used at the start of the phase analysis procedure (after subtraction of the background) to define the amount (in counts) of sulphate present. With knowledge of the complete pattern for $PbSO_4$, the amount (in counts) of α-PbO_2 in the sample was determined by subtracting appropriate numbers of $PbSO_4$ counts from the total counts accumulated in scanning ranges 2, 4, and 6 (Table 1). The amount (in counts) of β-PbO_2 was in turn determined by subtracting appropriate numbers of α-PbO_2 and/or $PbSO_4$ counts from scanning ranges 3, 5 and 7. The net counts for each phase were then normalized by the NC_i values and weight percentages were determined by eqn. (2).

Analysis of calculated patterns

Although pooling the intensities of four peaks from each phase serves to minimize the effects of preferred orientation, the need to undertake a certain amount of peak stripping because of the presence of severe peak overlapping means that detailed prior knowledge of the relative intensities of reflections from each phase in the scan is necessary. Here, the calculated patterns in Fig. 1 are particularly important since they both provide theoretical intensities (Table 1) and illustrate the effects of several potential diffraction problems.

For example, in Fig. 1(b), *HW* has been doubled relative to the value used in Fig. 1(a), an effect that would be produced by a significant reduction in particle size. This causes a corresponding reduction in the peak height, but the integrated peak area (as measured by the normalization constant) remains identical, illustrating the futility of using the diffraction peak height to estimate phase abundance. On the other hand, the normalization constant and the α-PbO_2 peak height increase dramatically when the presence of moderately severe preferred orientation about zone [100] in α-PbO_2 is modelled by increasing *PO* to 0.4 (Fig. 1(c)). The presence of structural disorder in α-PbO_2 is simulated in Fig. 1(d) by imposing a *BO* value of 5.0 on all atoms in this phase. As a result, the peak areas (and the *NC* value) have decreased by 23%, and the α-PbO_2 content of the mixture will therefore be overestimated by the same amount. The presence of an extreme level of non-stoichiometry has been modelled in Fig. 1(e) by using an *OC* value of 0.9 for α-PbO_2. In this case, the *NC* value drops by 19%, and the α-PbO_2 content will again be overestimated.

With these theoretical diffraction patterns available for comparison, and with a knowledge of how the patterns are affected by a variety of diffraction problems, it has been possible to carefully scrutinize various samples of PbO_2 and $PbSO_4$ in order to determine the degree of both crystallinity and phase purity as well as the presence of any preferred orientation. Several commercially available samples of β-PbO_2 and $PbSO_4$, together with α-PbO_2 prepared by oxidation of β-PbO at 340 °C [66] and α- and β-PbO_2 prepared by electroformation of positive battery plates in 1M NaOH and 4M H_2SO_4, respectively, were submitted to different periods of mechanical grinding and then subjected to X-ray analysis. Only in the case of β-PbO_2 did prolonged grinding produce any observable change in the diffraction pattern, and this involved the appearance of small amounts of α-PbO_2, no doubt produced in response to intermittent regions of high pressure in the ball mill. For all samples of β-PbO_2 and $PbSO_4$, and for chemically prepared α-PbO_2, the integrated observed peak intensities agreed satisfactorily with the calculated values (Table 1). However, compared with the diffraction patterns from chemically prepared α-PbO_2, the patterns from α-PbO_2 prepared by electroformation in 1M NaOH had much higher backgrounds and displayed small differences in peak positions and intensities. The latter behaviour can be related primarily to a small change in the y coordinate and the site occupancy of the Pb atom in the α-PbO_2 structure [70]. Although

pertinent to the overall discussion, the small differences observed for electroformed α-PbO_2 can be considered to be extreme since the alkaline synthesis was invoked in order to obtain *pure* α-PbO_2 and thus was not performed under the conditions encountered in normal battery manufacture and operation, *i.e.*, a sulphuric acid electrolyte.

Normalization constants for α-PbO_2 and $PbSO_4$ in 50:50 (by weight) binary mixtures with β-PbO_2, using Univar AR β-PbO_2 as the reference phase (*NC* = 1.0), are given in Table 2. Similar results were observed for corresponding binary mixtures of α-PbO_2 and $PbSO_4$ with electroformed β-PbO_2. Whereas *NC* values obtained for $PbSO_4$ from different commercial sources were close to the calculated normalization constant, a wide range of values was observed for α-PbO_2 samples prepared either by chemical oxidation of β-PbO or by electroformation in 1M NaOH.

The normalization constants for chemically prepared α-PbO_2 were always greater than the calculated value. This result disagrees with the conclusions of other workers [64, 72], who maintain that α-PbO_2 displays an "abnormally low intensity" (and hence a low *NC* value) in mixtures with β-PbO_2. Since the β-PbO_2 sample used as the reference phase produced satisfactory agreement between the observed and calculated *NC* values for $PbSO_4$, the high observed *NC* values for chemically prepared α-PbO_2 must be related to slight effects from micro-absorption, extinction, or residual preferred orientation in this variety of dioxide. On the other hand, binary mixtures of electrochemically prepared samples of α-PbO_2 with β-PbO_2 gave a range of *NC* values well below that obtained by calculation*.

TABLE 2

Observed and calculated normalization constants (*NC*) for α-PbO_2 and $PbSO_4$ in 50:50 (by weight) mixtures with Univar Analytical Reagent β-PbO_2

Compound	(hkl)[a]	NC_{obs}	NC_{calc}
$PbSO_4$[b]	(210) + (121)	0.50 - 0.53	0.50
α-PbO_2[c]	(111) + (020)	1.38 - 1.60	1.24
α-PbO_2[d]	(111) + (020)	0.51 - 0.68	1.12

[a]The reflections listed arbitrarily define *NC* in terms of the most intense peaks of each phase relative to the (011) reflection of β-PbO_2 (Table 1).
[b]Commercial Unilab and BDH Laboratory Reagents.
[c]Prepared by oxidation of β-PbO at 340 °C [66].
[d]Prepared by electroformation in 1M NaOH.

*Note that the calculated *NC* value given in Table 2 for electroformed α-PbO_2 is slightly smaller than that for chemically prepared α-PbO_2. This is a result of small structural differences between the two varieties, as mentioned earlier.

As discussed above in relation to Fig. 1, this variation in experimental *NC* values can be attributed to electrochemically prepared α-PbO_2 having one or more of the following characteristics: (i) an amorphous content of up to 50%; (ii) structural disorder to an extent much greater than the level simulated in Fig. 1(d); (iii) a lead deficiency greater than that modelled in Fig. 1(e). The high background levels for electroformed α-PbO_2 relative to chemically prepared material, together with the results of neutron diffraction structural studies currently in progress in our laboratory [70], suggest that the first of these possibilities is the most likely.

The marked variation of α-PbO_2 normalization constants on both sides of the calculated value confirms our decision to use calculated peak intensities and normalization constants in the phase analyses. The calculated values of these parameters were obtained from an X-ray single-crystal structure refinement in the case of $PbSO_4$ [71], and from an analysis of the neutron powder diffraction pattern from only the well crystallized material in the case of the lead dioxides [70]. In this way, we have avoided the uncertainty associated with micro-absorption, preferred orientation, degree of crystallinity, level of non-stoichiometry, structural disorder, etc., that is present when calibration is based on the selection of a particular "standard" material. Under these circumstances, the phase analysis results apply only to the crystalline components in samples collected from batteries. Estimations of the amounts, and studies of the properties, of amorphous material that may be present in positive plates will be reported elsewhere.

Accuracy and precision of the analytical method

Determining the accuracy of the phase analysis technique is difficult in the case of samples containg α-PbO_2 since this material is of variable quality and has observed *NC* values that are known to be significantly different from the corresponding calculated values. Nevertheless, since the *NC* value calculated for chemically prepared α-PbO_2 differs by only 10% from the *NC* value calculated for α-PbO_2 prepared by alkaline electroformation (Table 2), one might expect that the maximum uncertainty in the calibration constant for this material is of that order. For a sample containing about 50% (by weight) of α-PbO_2, the resulting phase composition would therefore be in error by a maximum of about 5 wt.%.

The good agreement between the calculated and observed *NC* values for $PbSO_4$ suggests that β-PbO_2 and $PbSO_4$ compositions can be determined more accurately than the composition of α-PbO_2. Indeed, analyses of selected binary mixtures of β-PbO_2 with $PbSO_4$ have shown that the calculated phase compositions are within about 3 wt.% of their real values. Moreover, repeated analyses of samples prepared by different operators using different mounting methods, sample thicknesses, grinding times, and step-counting times have given results that are reproducible to within 2% (by weight) for all three phases in ternary mixtures.

Experimental

Batteries were subjected to charge/discharge cycles that simulated service in an electric vehicle. This was achieved with equipment specially designed and constructed in our laboratory [73, 74]. The discharge current was established from measurements with a test vehicle driven over a standard course.

The driving profile selected for the test vehicle was the one developed by the Australian Electric Vehicle Association (AEVA) [75]. The AEVA profile typifies the demands placed on a vehicle in an urban environment and consists of a schedule of accelerations, constant speeds, decelerations, and idle intervals (Fig. 2). The speed and time for each operation are defined. The total time for one cycle is 120 s, the maximum speed is 60 km/h, the average speed is 30 km/h, and the distance travelled is 1 km. The AEVA profile is similar to standard profiles that have become part of the legislated emission and fuel-consumption control procedures for internal combustion engine vehicles in various countries *e.g.*, the European ECE 15 Test, the 1976 Japanese 11-Mode Test, etc. The profiles are believed to represent typical driving patterns and have been developed only after detailed analysis of data for a wide range of vehicles, experimental methods, and test routes.

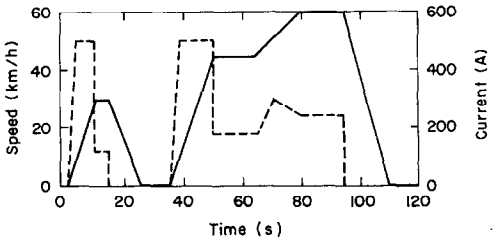

Fig. 2. AEVA urban driving profile (——) and the corresponding battery current approximation (– – –) for the Battronic electric van.

A Battronic electric van was used as the test vehicle. The van was built by the Boyertown Auto Body Works in Pennsylvania and is powered by fifty-six 2 V/350 A h (6 h rate) traction cells supplied by Dunlop Batteries Australia. In order to determine the power characteristics of the van during operation according to the AEVA profile, we installed instruments to measure road speed, battery voltage, and current. Tests were performed over a 1 km stretch of level public road near our laboratory. The current profile experienced by the van during operation is shown in Fig. 2. Each road test was terminated when the vehicle was no longer able to meet the acceleration requirements of the driving profile; this occurred at a battery voltage corresponding to ~1.6 V per cell.

In the laboratory simulation experiments, the charge/discharge cycling procedure was as follows: (i) the battery was charged at a constant current of 10 A, followed by a crossover to constant voltage control at 15.3 V, with charge termination 3 h after a voltage of 14.4 V had been

reached; (ii) the battery was discharged following the Battronic van current–time profile over the AEVA duty cycle, using smooth-current discharge; (iii) a switch to charging was made when the terminal voltage fell below that found necessary in the Battronic van to maintain the power requirements of the driving profile, *viz.*, 9.6 V; (iv) an equalizing charge for 6 h beyond 14.4 V was provided every eighth cycle, *i.e.*, after seven complete charge/discharge cycles. The procedure was repeated until the battery was considered to have reached the end of its useful operational life. This condition was arbitrarily chosen as the point at which the discharge capacity, converted to the 20 h rate, had declined to 75% of the nominal value provided by the manufacturer.

TABLE 3

Characteristics of lead/acid batteries

Battery	Grid Sb content (wt.%)		Positive paste density (kg/l)	Nominal capacity at 20 h rate (A h)	End-of-life capacity at nominal rate (A h)	Capacity at average AEVA rate (A h)	End-of-life capacity at average AEVA rate (A h)
	Positive plate	Negative plate					
Test							
T1	5.9	6.3	4.09	60.0	45.0	28.6	19.5
T2, T3	5.9	6.3	4.31	54.2	40.7	25.0	17.1
T4, T5	4.1	5.5	4.58	50.0	37.5	22.6	15.4
Golf-cart							
C1	5.0	5.2	—	220.0	165.0	104.7	71.6

The above charge/discharge cycling experiments were carried out both on test batteries provided by Dunlop Batteries Australia and on commercial "golf-cart" systems produced in the United States; battery parameters are listed in Table 3. Since each of these batteries has a smaller capacity than that of the batteries in the Battronic van, the discharge current profile under laboratory conditions was scaled down by a factor equal to the ratio of the test-battery capacity to the vehicle-battery capacity. Table 3 also gives the initial and "end-of-life" capacities of the test and golf-cart batteries at a rate corresponding to discharge at the calculated average current for the corresponding scaled-down AEVA profile.

Both the test and the golf-cart batteries consisted of two 6 V modules joined in series. The test cells contained 9 plates (4 positive, 5 negative), and the golf-cart cells contained 19 plates (9 positive, 10 negative). The positive plates in both systems were placed in fibreglass envelopes. The test battery plates were housed in two 3-cell, clear styrene acrylonitrile containers with detachable lids and specially designed intercell connectors [74]. This arrangement allowed the test batteries to be disassembled easily for collecting plate specimens at various stages of cycle life. The golf-cart batteries, on the other hand, were supplied in sealed containers and could

not be periodically opened for inspection. However, samples were collected from uncycled units (which were thereby rendered unsuitable for service), and cell autopsies were carried out on failed batteries.

Since samples were obtained by completely removing 1 cm square blocks of material from the central region of the plates, the XRD measurements provide a phase analysis for the full cross-section of each plate. At this stage, no attempt has been made to achieve a depth analysis across the thickness of the plates. The samples were washed with distilled water, the grid pieces removed, and the remaining bulk active material ground in an agate mortar under alcohol. The damp mass was then floated onto a ground-glass substrate and allowed to dry by evaporation. X-ray intensities for the nine scanning regions and two background positions were collected with copper $K\alpha_1$ radiation in a standard Philips diffractometer fitted with a curved graphite monochromator and a 2θ stepping motor interfaced to a teletype. A step width of 0.01° and a step counting time of 0.4 s were employed. These correspond to a continuous scanning rate of 1.5° min and an analysis time of about 30 min per sample.

Results and discussion

Battery performance

The performance of several batteries subjected to AEVA charge/discharge cycling is shown in Table 4. These results are representative of studies carried out in our laboratory on many other similar batteries. The golf-cart battery (C1) gave by far the best performance — the service life was much greater than that of the test battery (T4) with the nearest positive plate composition. The data obtained on the test batteries showed that elevation of the operating temperature improved the cycle life (*cf.* the performance of batteries T2 and T3, Table 4). Removal of the fibreglass envelopes around the positive plates markedly reduced the cycle life (*cf.* the performance of batteries T4 and T5) because of accelerated shedding of positive active material.

Phase analyses of the positive plates showed that the degree to which the active material was utilized depended on both the paste density and the operating temperature. Increasing the paste density decreased the utilization, whereas elevating the operating temperature improved the discharge capacity, particularly with the denser plates. In any event, the maximum utilization of positive active material did not exceed 45%.

XRD analysis of "sludge" collected from the bottom of each cell showed that the amount of $PbSO_4$ shed from batteries cycled at 40 °C was greater than that from batteries cycled at 25 °C. This behaviour may be the result of an increase in the crystal size of $PbSO_4$ in batteries cycled at the higher temperature [76].

TABLE 4

Quantitative XRD analyses of the crystalline phases of positive plates in lead/acid batteries subjected to simulated electric-vehicle service: major trends for the batteries studied

Battery	Test temperature (° C)	Initial α-PbO_2:β-PbO_2 ratio	Cycle life (AEVA cycles)	α-PbO_2:β-PbO_2 ratio at failure (charged plate)	Mean α-PbO_2:β-PbO_2 ratio in grid skins
T1	25	0.21	49	0.04	0.33 (cycle 26)
T2	25	0.30	117	0.08	0.31 (cycle 235)
T3	40	0.31	145	0.07	—
T3 (repasted)	40	0.15	50	0.09	—
T4	25	0.61	160	0.24	—
T5	25	0.61	89[a]	0.24	0.29 (cycle 100)
C1	25	1.07	431	0.36	0.67

[a]Positive plates not enclosed in fibreglass envelopes.

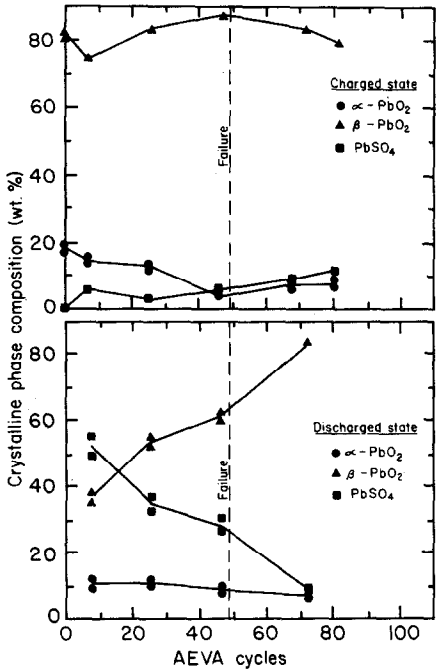

Fig. 3. Crystalline phase composition (wt.%) of charged and discharged positive plates from test lead/acid battery T1 (paste density = 4.09 kg/l) after AEVA cycling at 25 °C with smooth-current discharge. Lines are drawn through the average of multiple measurements at a given cycle.

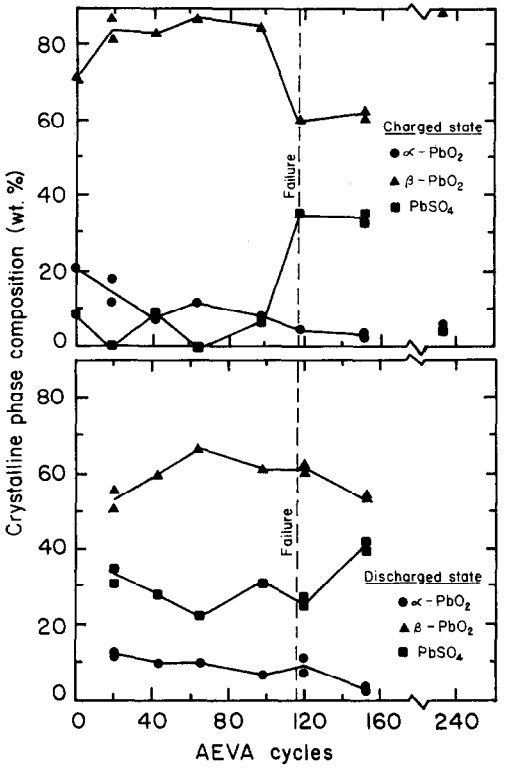

Fig. 4. Crystalline phase composition (wt.%) of charged and discharged positive plates from test lead/acid battery T2 (paste density = 4.31 kg/l) after AEVA cycling at 25 °C with smooth-current discharge. Lines are drawn through the average of multiple measurements at a given cycle.

α-PbO_2:β-PbO_2 ratio and cycle life

The influence of positive-plate phase composition on battery performance was studied by subjecting test batteries containing different initial α-PbO_2:β-PbO_2 ratios to the same charge/discharge cycling conditions. The ratio was varied first by increasing the paste density (batteries T2 and T3) and also by using less acidic charging conditions during plate formation (batteries T4 and T5). As explained above, both of these factors enhance the formation of α-PbO_2. The data presented in Table 4 for batteries T1, T2 and T4 show that a correlation exists between battery cycle life and the initial relative amounts of α- and β-PbO_2 in the positive plate, *i.e.*, battery performance is significantly improved by increasing the initial proportion of α-PbO_2. Since Dodson [40] found that increasing the α-PbO_2 content produced only a slight improvement in performance under low-rate discharge conditions, the results presented here suggest that the α-PbO_2 content is more important under the more severe conditions of traction service.

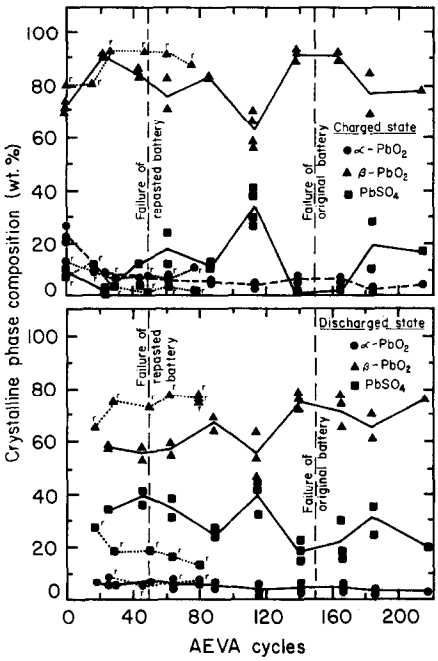

Fig. 5. Crystalline phase composition (wt.%) of charged and discharged positive plates from test lead/acid battery T3 (paste density = 4.31 kg/l) after AEVA cycling at 40 °C with smooth-current discharge. Data labelled with the letter *r* are for the same battery after repasting. Lines are drawn through the average of multiple measurements at a given cycle.

The test batteries showed a consistent decrease in the α-PbO_2:β-PbO_2 ratio during charge/discharge cycling, irrespective of the operating temperature (Figs. 3 - 6). This decrease is not the result of actual shedding of oxide, for analysis of the battery sludge showed that the proportion of α-PbO_2 in the shed material is at all stages of battery life lower than that in the bulk mass of the plate. This observation supports previous findings [36, 47 - 50] that α-PbO_2 forms a resilient, skeletal framework within the plate active mass, thereby minimizing the amount of material lost through shedding. The change in the α-PbO_2:β-PbO_2 ratio is therefore predominantly the result of conversion of some of the α-PbO_2 to $PbSO_4$ during discharging, followed by reconversion of part of this $PbSO_4$ to β-PbO_2 during charging. The conversion of α-PbO_2 to β-PbO_2 is particularly rapid during the first 30 or so cycles of battery life (Figs. 3 - 6). The α-PbO_2 content then levels off at about half the initial amount present in the bulk active material. Note that since it was impractical to sample the same plate (or all plates) every few cycles, the analyses shown in Figs. 3 - 6 are for different plates and cells in a given battery. Further investigations have shown that each

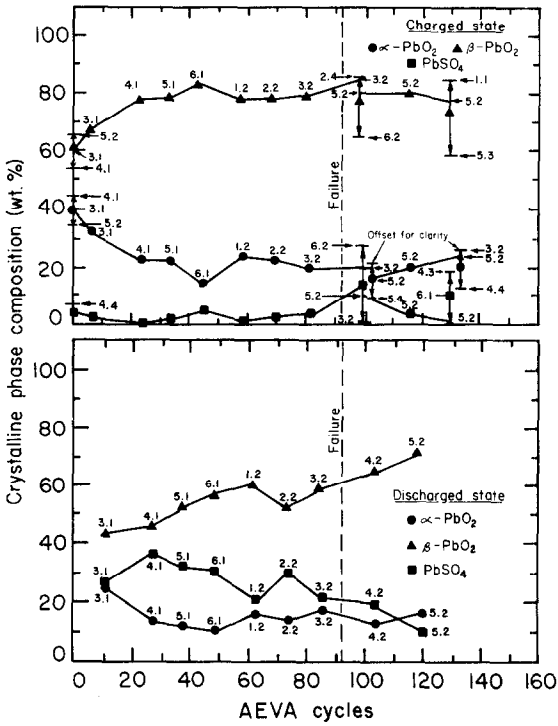

Fig. 6. Crystalline phase composition (wt.%) of charged and discharged positive plates from test lead/acid battery T5 (paste density = 4.58 kg/l) after AEVA cycling at 25 °C with smooth-current discharge. At cycles 1, 100, and 130, the composition ranges for all 24 plates in the battery are shown, together with specific values for some individual samples. The origin of each sample is indicated by a cell and plate number, *e.g.*, "1.2" represents cell 1, plate 2. Lines are drawn to connect measurements for the same plate, or for the corresponding plate in a following cell.

plate develops its own unique charge/discharge characteristics (see below), so trends in phase composition rather than absolute magnitudes for individual plates should be used in considering the data presented in Figs. 3 - 6.

Battery T5 was heavily sampled in order to ascertain the range of compositions to be expected in an individual plate, and to monitor changes more frequently as a function of cycle life. All 24 positive plates of the battery were sampled after (i) initial charging; (ii) 100 cycles, *i.e.*, just following failure*; (iii) 130 cycles. The results are given in Table 5 and

*This battery (T5) was used to investigate the effects of shedding of positive active material on cycle life and so did not have fibreglass envelopes around its positive plates. Thus, failure occurred more rapidly than in the case of batteries having a similar positive paste composition but with fibreglass-covered plates, *cf.* the cycle lives of batteries T4 and T5, Table 4.

TABLE 5

Ranges of bulk active-material compositions (wt.%) for the four positive plates in each of the six cells of battery T5 at various stages of cycle life

Cell no.	Initial charge			100 cycles			130 cycles		
	α-PbO_2	β-PbO_2	$PbSO_4$	α-PbO_2	β-PbO_2	$PbSO_4$	α-PbO_2	β-PbO_2	$PbSO_4$
1	39 - 41	59 - 62	0	12 - 18	81 - 84	0 - 6	12 - 16	73 - 83	5 - 12
2	36 - 42	58 - 64	0 - 0.4	12 - 19	75 - 85	2 - 12	14 - 23	75 - 80	0 - 11
3	41 - 45	55 - 59	0	11 - 20	79 - 82	0 - 7	20 - 26	70 - 72	3 - 10
4	41 - 45	55 - 59	0 - 1	9 - 18	66 - 80	6 - 23	11 - 17	68 - 76	11 - 18
5	34 - 40	60 - 66	0	8 - 22	67 - 76	5 - 25	19 - 24	60 - 77	0 - 18
6	35 - 41	59 - 65	0	9 - 14	64 - 83	8 - 27	13 - 18	71 - 75	10 - 16
Max.–min. limits	34 - 45	55 - 66	0 - 1	8 - 22	64 - 85	0 - 27	11 - 26	60 - 83	0 - 18

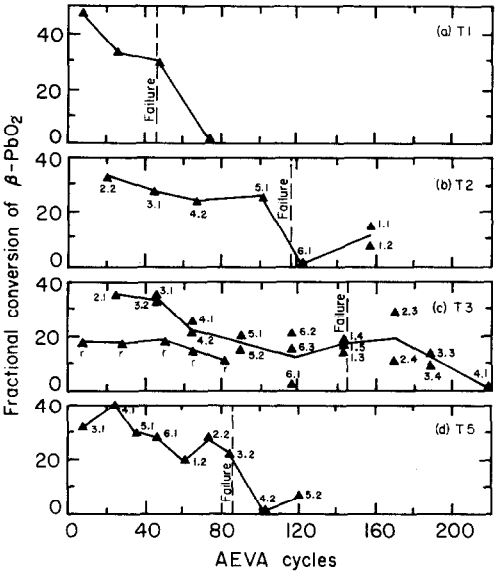

Fig. 7. Fractional conversion (%) of β-PbO_2 to $PbSO_4$ upon charge/discharge for various test lead/acid batteries after AEVA cycling with smooth-current discharge. The origin of each sample is indicated by a cell and plate number, *e.g.*, "1.2" represents cell 1, plate 2. Data labelled with the letter *r* are for battery T3 after repasting. Lines are drawn through the average of multiple measurements at a given cycle.

Fig. 6. Individual plates developed their own unique phase compositions as the battery was cycled, presumably as a result of small variations in the initial paste composition and density, grid surface area, etc. Cells 4 - 6, in the second of the two 6 V containers of the 12 V assembly, had significantly higher levels of $PbSO_4$ after 100 cycles than cells 1 - 3 in the first container. It is difficult to explain this result since the cells were all connected in series. However, continued cycling of the battery resulted in reconversion

of the $PbSO_4$ to β-PbO_2 so that, after 130 cycles, cells 4 - 6 more closely resembled cells 1 - 3. This variability between plates can also be seen in single samples taken approximately every 10 cycles throughout battery operation (Fig. 6), and in plots of the fractional conversion of β-PbO_2 to $PbSO_4$ (Fig. 7). From these analyses, it is apparent that failure occurs when one or more of the plates is converting little (or no) dioxide to sulphate, despite the fact that other plates may still have high conversion rates (*e.g.*, plates 1.1 and 2.3 in batteries T2 and T3, respectively, Fig. 7). Some plates therefore appear to be more "active" than others and may carry out the bulk of the work.

A more detailed study of the relative behaviour of α-PbO_2 and β-PbO_2 could be made with battery T5 since this battery contained a large initial quantity of α-PbO_2. As stated earlier, the youthful stages of battery life (cycles 0 - 30) are characterized by a rapid decrease in the amount of α-PbO_2 in the bulk active material and a corresponding increase in the β-PbO_2 content (Fig. 6). During this stage, about 35% of the β-PbO_2 content (Fig. 7(d)) and about 20% of the α-PbO_2 content are converted to $PbSO_4$; this represents only about 25% utilization of the total active mass. All of the $PbSO_4$ formed from β-PbO_2, and essentially all of that formed from α-PbO_2, is converted back to β-PbO_2. This situation changes after about 30 cycles, when the amount of α-PbO_2 in the charged active mass reaches an approximately constant value of around 20 wt.% (Fig. 6). For some time after this, *i.e.*, until about cycle 80, about one-quarter of the α-PbO_2 continues to be converted during discharging, but now it is regained on subsequent charging rather than undergoing conversion to the β-form. This behaviour probably reflects the fact that the reactions in the initial and latter stages of cycle life take place at different locations in the plate (*i.e.*, α-PbO_2 converted to $PbSO_4$ on the exterior of the plate is converted back to β-PbO_2 in the lower pH environment there, while α-PbO_2 converted to $PbSO_4$ in the interior of the plate re-forms to α-PbO_2 in the higher pH environment near the grid). When there is no longer any α-PbO_2 on the plate exterior to be lost to β-PbO_2 on charge/discharge cycling, only the reversible conversion to $PbSO_4$ takes place and thenceforth the α-PbO_2 content remains constant in the bulk material.

Analysis of corrosion-layer material — scraped from the alloy grid after removal of the loosely adhering paste — shows that throughout battery cycle life the α-PbO_2 content in the grid skins remains high (Table 4). This further supports the suggestion that the α-PbO_2 on the interior of the plate is reversibly converted to $PbSO_4$ during battery discharge.

After about the 80th cycle of the battery T5, no further conversion of α-PbO_2 to $PbSO_4$ occurred (Fig. 6). This may represent either the entrapment of the residual α-PbO_2 particles by large $PbSO_4$ or β-PbO_2 crystals, or the development of an electrochemically inactive form of α-PbO_2 similar to that proposed [27 - 29] for β-PbO_2.

Mode of battery failure

As shown above for battery T5 (Fig. 6) and other batteries (Figs. 3 - 5), the fraction of PbO_2 (both α and β) converted to $PbSO_4$ upon discharge was around 20 to 40% during initial service and approached 0% on cycling beyond battery failure. These figures correspond reasonably well with the measured capacities. Throughout the useful battery life, $PbSO_4$ continued to be converted back to β-PbO_2 during charging, indicating a maintenance of electrical contact between the grid and the bulk active material. Thus, the active mass in the discharged condition gradually assumed the composition of a charged battery plate, *i.e.*, high β-PbO_2 and low $PbSO_4$. This suggests that although the β-PbO_2 active mass was in electrical contact with the grid, it was eventually unable to be discharged and could have been converted into an electrochemically inactive form as proposed by Caulder *et al.* [27 - 29].

The poor cycle life of lead/acid batteries under deep-discharge conditions has also been attributed [77 - 79] to the build-up of a lead sulphate "barrier layer" at the grid/active material interface. Since scanning electron microscope and electron microprobe investigations in our laboratory have provided evidence for such a mechanism [73, 74], an experiment was performed to determine whether battery failure is due to passivation of the grids or passivation of the active material. This involved carefully removing the active material from the positive grids of a battery (T3) at failure and repasting the same grids with fresh paste. The new plates were formed, reconstructed into a new battery with a fresh set of negative plates, and subjected to the same AEVA cycling conditions (40 °C, smooth-current discharge) as their predecessors.

The capacity of the battery was partially regained (Fig. 5), indicating that either (i) the original failure was caused by the formation of electrochemically inactive PbO_2 (replacement of this oxide returns capacity to the battery), or (ii) the original failure was caused by the formation of insulating/passivating corrosion layers on the grids (repasting disturbs these layers so that electrical contact with the active mass is restored).

The short cycle life and reduced capacity of the repasted battery are evidence against conclusion (i) (see Table 4). However, the α-PbO_2 content of the repasted battery was about half that of the original. This is almost certainly a consequence of different paste densities since the plates in the reconstructed battery were prepared by hand rather than by machine. Although a reduction in the α-PbO_2 content has an adverse effect on cycle life, the amount of PbO_2 converted to $PbSO_4$ during discharge of the repasted battery was, *from the outset*, consistently lower (by a factor of about two, Fig. 5) than it was for the original battery. This observation supports conclusion (ii) above, *i.e.*, that the original battery failure was due to passivation of the grid. After a short period, the exposed portions of the grid in the repasted battery appear to become re-passivated and failure occurs.

Conclusions

XRD phase analysis of the positive-plate active material of lead/acid batteries operated under simulated traction service has shown that less than 45% of this material is utilized during discharge and that this conversion rate falls soon after the battery is cycled.

Individual positive plates develop their own unique phase compositions during battery service, with the α-PbO_2:β-PbO_2 ratio decreasing on continuous charge/discharge cycling. This is because of the gradual conversion of α-PbO_2 to β-PbO_2 on the exterior of the plates *via* the $PbSO_4$ formed upon discharge. Very little α-PbO_2 is lost through the shedding of active material. The α-PbO_2:β-PbO_2 ratio in the positive plate exerts a marked influence on battery cycle life — performance is improved by increasing the initial proportion of α-PbO_2.

The failure of only a few positive plates is sufficient to terminate useful battery life. The main cause of plate failure in the test batteries has not yet been identified, but XRD analyses of repasted, aged grids strongly suggest that grid passivation by sulphate films is a key factor. Other phenomena contributing to loss of battery capacity include electrochemical inactivation of both α- and β-PbO_2 and breakdown of the α-PbO_2 microstructure.

XRD analyses of positive plates showed that the amount of $PbSO_4$ shed from batteries cycled at 40 °C is greater than that shed from batteries cycled at 25 °C. However, since indications are that increasing the operating temperature improves the cycle life, it is likely that shedding is not the major cause of battery failure at elevated temperatures.

Acknowledgements

We are indebted to the Australian Lead Development Association for the loan of their Battronic electric van; to Dunlop Batteries Australia for supplying materials for the test batteries; to the International Lead Zinc Research Organization for their joint support and for permission to publish this work; and to our colleagues J. A. Hamilton, I. C. Madsen, J. F. Moresby, and P. R. Strode for assistance in the experimental work.

References

1 W. Mindt, *J. Electrochem. Soc., 116* (1969) 1076.
2 N. Kameyama and T. Fukumoto, *J. Soc. Chem. Ind. Jpn., 49* (1946) 1946.
3 E. V. Krivolapova and B. N. Kabanov, *Trudy Soveshch. Elektrokhim. Akad. Nauk SSSR, Otd. Khim. Nauk, 1950* (1953) 539.
4 I. A. Bagotzkaya and A. N. Frumkin, *Dokl. Akad. Nauk SSSR, 92* (1953) 979.
5 B. N. Kabanov, I. G. Kiseleva and D. I. Liekis, *Dokl. Akad. Nauk SSSR, 99* (1954) 805.
6 J. Burbank, *J. Electrochem. Soc., 103* (1956) 87.
7 J. Burbank, *J. Electrochem. Soc., 104* (1957) 693.

8 P. Ruetschi and B. D. Cahan, *J. Electrochem. Soc., 104* (1957) 406.
9 P. Ruetschi and B. D. Cahan, *J. Electrochem. Soc., 105* (1958) 369; *106* (1959) 1079.
10 E. V. Krivolopova, E. S. Wiesberg and B. N. Kabanov, *Trans. 4th Electrochem. Meeting,* Akad Nauk SSSR, Moscow, 1959, p. 757.
11 S. Ikari, S. Yoshizawa and S. Okadi, *Denki Kagaku, 27* (1959) 487; *J. Electrochem. Soc. Jpn., Overseas Edn., 27* (1959) E-186.
12 I. I. Astakhov, E. S. Vaisberg and B. N. Kabanov, *Dokl. Akad. Nauk SSSR, 154* (1964) 1414; *Am. Soc. Met. Rev. Met. Lit., 21* (1964) Abstr., p. 45.
13 B. N. Kabanov, E. S. Weisberg, I. L. Romanova and E. V. Krivolapova, *Electrochim. Acta, 9* (1964) 1197.
14 D. Pavlov, *Ber. Bunsenges., 71* (1967) 398.
15 D. Pavlov, *Electrochim. Acta, 13* (1968) 2051.
16 D. Pavlov, C. N. Poulieff, E. Klaja and N. Iordanov, *J. Electrochem. Soc., 116* (1969) 316.
17 D. Pavlov and N. Iordanov, *J. Electrochem. Soc., 117* (1970) 1103.
18 E. M. L. Valeriote and D. Gallop, *J. Electrochem. Soc., 124* (1971) 370.
19 P. Ruetschi, *J. Electrochem. Soc., 120* (1973) 331.
20 I. A. Aguf, *Khim. Istockikam, SSSR, 10* (1975) 34.
21 M. A. Dasoyan and I. A. Aguf, *Current Theory of Lead–Acid Batteries,* Technicopy, Stonehouse, England, 1979, pp. 234 - 241.
22 B. K. Mahato, *J. Electrochem. Soc., 126* (1979) 365.
23 H. Bode and E. Voss, *Z. Elektrochem., 60* (1956) 1053.
24 V. H. Dodson, *J. Electrochem. Soc., 108* (1961) 401.
25 D. Kordes, *Chem. Ing.-Tech., 38* (1966) 638.
26 S. M. Caulder and A. C. Simon, *J. Electrochem. Soc., 121* (1974) 1546.
27 S. M. Caulder, J. S. Murday and A. C. Simon, *J. Electrochem. Soc., 120* (1973) 1515.
28 A. C. Simon and S. M. Caulder, in D. H. Collins (ed.), *Power Sources 5,* Academic Press, London, 1975, p. 109.
29 A. C. Simon, S. M. Caulder and J. T. Stemmle, *J. Electrochem. Soc., 122* (1975) 461.
30 E. Voss and J. Freundlich, in D. H. Collins, (ed.), *Batteries,* Pergamon Press, Oxford, 1963, p. 73.
31 W. C. M. Carey, X-ray diffraction as a technique for studying lead–acid battery plates, *Rep. C. R. 21, July 1965,* British Railways Research Department.
32 N. E. Bagshaw and K. P. Wilson, *Electrochim. Acta, 10* (1965) 867.
33 I. Dugdale, in D. H. Collins (ed.), *Power Sources 1966,* Pergamon Press, Oxford, 1967, p. 142.
34 W. A. Butler, C. J. Venuto and D. V. Wisler, *J. Electrochem. Soc., 117* (1970) 1339.
35 J. Armstrong, I. Dugdale and W. J. McCusker, in D. H. Collins (ed.), *Power Sources 1966,* Pergamon Press, Oxford, 1967, p. 163.
36 A. C. Simon and E. J. Jones, *J. Electrochem. Soc., 109* (1962) 760.
37 P. Ruetschi and R. T. Angstadt, *J. Electrochem. Soc., 111* (1964) 1323.
38 D. Pavlov, G. Popazov and V. Iliev, *J. Electrochem. Soc., 118* (1972) 8.
39 S. Ikari, S. Yoshizawa and S. Okada, *Denki Kagaku, 27* (1959) 552; *J. Electrochem. Soc. Jpn., Overseas Ed., 27* (1959) E-223.
40 V. H. Dodson, *J. Electrochem. Soc., 108* (1961) 406.
41 H. B. Mark, Jr., *J. Electrochem. Soc., 109* (1962) 634.
42 R. I. Angstadt, C. J. Venuto and P. Reutschi, *J. Electrochem. Soc., 109* (1962) 177.
43 P. Ruetschi, J. Sklarchuk and R. T. Angstadt, in D. H. Collins (ed.), *Batteries,* Pergamon Press, Oxford, 1963, p. 89; *Electrochim. Acta, 8* (1962) 333.
44 D. Berndt and E. Voss, in D. H. Collins (ed.), *Batteries 2,* Pergamon Press, Oxford, 1965, p. 17.
45 J. R. Pierson, *J. Electrochem. Technol., 5* (1967) 323.
46 K. Wiesener, W. Hoffman and O. Rademacher, *Electrochim. Acta, 18* (1973) 913.
47 A. C. Simon, in D. H. Collins (ed.), *Batteries 2,* Pergamon Press, Oxford, 1965, p. 63.

48 J. Burbank, *J. Electrochem. Soc., 113* (1966) 10.
49 J. Burbank and E. J. Ritchie, *J. Electrochem. Soc., 116* (1969) 125.
50 T. J. Hüghel and R. H. Hammar, in D. H. Collins (ed.), *Power Sources 3*, Oriel Press, Newcastle upon Tyne, 1971, p. 35.
51 S. Hattori, M. Yamaura, M. Kono, M. Yamane, N. Nakashima and J. Yamashita, *ILZRO Project LE-276, Progress Report No. 2*, December 1, 1977 - November 30, 1978, International Lead Zinc Research Organization, Inc.
52 P. Ness, *Electrochim. Acta, 12* (1967) 161.
53 T. Chiku, *J. Electrochem. Soc., 115* (1968) 981.
54 D. Pavlov, V. Iliev, G. Papazov and E. Bashtavelova, *J. Electrochem. Soc., 121* (1974) 854.
55 K. Wiesener and P. Reinhardt, *Z. Phys. Chem., 256* (1975) 285.
56 J. R. Dafler, *J. Electrochem. Soc., 124* (1977) 1312.
57 P. R. Skidmore and R. R. Schwartz, *Analyst, 104* (1979) 952.
58 V. Iliev and D. Pavlov, *J. Appl. Electrochem., 9* (1979) 555.
59 L. Alexander and H. P. Klug, *Anal. Chem., 20* (1948) 886.
60 L. E. Copeland and R. H. Bragg, *Anal. Chem., 30* (1958) 196.
61 S. Popovic and B. Grzveta-Plenkovic, *J. Appl. Crystallogr., 12* (1979) 205.
62 B. L. Averbach and M. Cohen, *Trans. AIME, 176* (1948) 401.
63 F. H. Chung, *J. Appl. Crystallogr., 8* (1975) 17.
64 J. Burbank, A. C. Simon and E. Willihnganz, in P. Delahay and C. W. Tobias (eds.), *Advances in Electrochemistry and Electrochemical Engineering*, Wiley-Interscience, New York, 1971, p. 157.
65 B. D. Cullity, *Elements of X-Ray Diffraction*, Addison-Wesley, Reading, MA, 2nd Edn., 1978, p. 417.
66 N. E. Bagshaw, R. L. Clarke and B. Halliwell, *J. Appl. Chem., 16* (1966) 180.
67 J. A. Duisman and W. F. Giauque, *J. Phys. Chem., 72* (1968) 562.
68 H. M. Rietveld, *J. Appl. Crystallogr., 2* (1969) 65.
69 D. B. Wiles and R. A. Young, *J. Appl. Crystallogr., 14* (1981) 149.
70 R. J. Hill, Neutron powder diffraction profile refinements of the structures of chemically and electrochemically prepared samples of α- and β-PbO_2, to be published.
71 M. Miyake, I. Minato, H. Morikawa and S. Iwai, *Am. Mineral., 63* (1973) 506.
72 N. N. Federova, I. A. Aguf, L. M. Levinzon and M. A. Dasoyan, *Sb. Rab. Khim. Istochnikam Toka, 1966* (1966) 252.
73 D. Barrett, M. T. Frost, J. A. Hamilton, K. Harris, I. R. Harrowfield, J. F. Moresby and D. A. J. Rand, in D. A. J. Rand, G. P. Power and I. M. Ritchie (eds.), *Progress in Electrochemistry*, Elsevier, Amsterdam, 1981, p. 131.
74 J. R. Gardner, J. A. Hamilton, K. Harris, R. J. Hill, J. F. Moresby and D. A. J. Rand, *ILZRO Project LE-290, Prog. Rep. No. 4*, January - June 1981, International Lead Zinc Research Organization, Inc.
75 *Interim Procedure for Testing Electric Road Vehicles*, Australian Electric Vehicle Association, Melbourne, March 31, 1976.
76 M. T. Frost, J. A. Hamilton, K. Harris, I. R. Harrowfield, R. J. Hill, J. F. Moresby and D. A. J. Rand, *ILZRO Project No. LE-290, Prog. Rep. No. 3*, July - December 1980, International Lead Zinc Research Organization, Inc.
77 S. Tudor, A. Weistuch and S. H. Davang, *J. Electrochem. Technol., 3* (1965) 90; *4* (1966) 406; *5* (1967) 21.
78 S. Hattori, M. Yamaura, M. Kohno, M. Yamane, N. Nakashima and J. Yamashita, *ILZRO Project No. LE-253, Prog. Rep. for March - November, 1977*, International Lead Zinc Research Organization, Inc.
79 J. L. Weininger and E. G. Siwek, *J. Electrochem. Soc., 123* (1976) 602.